Astronomy
&
Astrophysics

Candidate stellar occultations by Centaurs and trans-Neptunian objects up to 2014[*,**,***,****]

J. I. B. Camargo[1], R. Vieira-Martins[1,2,†], M. Assafin[2], F. Braga-Ribas[1,3], B. Sicardy[3,4], J. Desmars[1],
A. H. Andrei[1,2,‡,§,¶], G. Benedetti-Rossi[1], and A. Dias-Oliveira[1,3]

[1] Observatório Nacional/MCTI, R. General José Cristino 77, CEP 20921-400 Rio de Janeiro, RJ, Brazil
   e-mail: camargo@linea.gov.br
[2] Observatório do Valongo/UFRJ, Ladeira do Pedro Antônio 43, CEP 20080-090 Rio de Janeiro, RJ, Brazil
   e-mail: massaf@astro.ufrj.br
[3] Observatoire de Paris-Meudon/LESIA, 5 place Jules Janssen, 92195 Meudon, France
[4] Université Pierre et Marie Curie, Institut Universitaire de France, Paris, France
   e-mail: bruno.sicardy@obspm.fr

Received 31 August 2013 / Accepted 29 October 2013

ABSTRACT

Context. We study trans-Neptunian objects (TNOs) from stellar occultations.
Aims. We predict stellar occultations from 2012.5 to the end of 2014 by 5 Centaurs and 34 TNOs.
Methods. These predictions were achieved in two ways: first, we built catalogues with precise astrometric positions of the stellar content around the paths on the sky of these targets, as seen by a ground-based observer; second, the observed positions of the targets were determined with the help of these same catalogues so that we could improve their ephemerides and the reliability of the predictions. The reference system is the International Celestial Reference System (ICRS) as realised by the Fourth US Naval Observatory CCD Astrograph Catalog (UCAC4). All the sky paths as well as the selected targets were observed from Oct. 2011 to May 2013 with the ESO/MPG 2.2 m telescope equipped with the Wide Field Imager (WFI). All astrometric results were obtained with the platform for reduction of astronomical images automatically (PRAIA) after correcting the images for overscan, bias, and flatfield.
Results. The catalogues with the stellar content around the sky path of each selected target are complete down to magnitude $R = 19$ and have an average positional accuracy of about 50 milliarcseconds. This same average accuracy also holds for the observed positions of the targets. In the catalogues from the sky paths, stellar proper motions for non-UCAC4 objects were derived from the combination of the current epoch WFI observations with either the 2MASS or the USNO-B1 catalogues. The offsets between the observed and (JPL) ephemeris positions of the targets frequently reach absolute values of some hundreds of milliarcseconds.
Conclusions. We present here stellar occultation predictions for the selected 5 Centaurs and 34 TNOs from 2012.5 to the end of 2014. This work is also an extension of two previous prediction works by us, the first one for Pluto, Charon, Nix, and Hydra, and the second for ten other large TNOs. The use of catalogues from the observations of the sky paths in the astrometry of the TNOs and Centaurs enhanced the coherence between their positions and those of the respective occulted candidate stars. New observations of these TNOs and Centaurs are continuously used to redetermine their ephemerides.

Key words. astrometry – occultations – Kuiper belt: general

---

1. Introduction

Trans-Neptunian objects (TNOs) constitute a population of small planetary bodies orbiting beyond Neptune, in a vast region (the Kuiper belt) extending to the outskirts of our solar system. They are observed as far as 30–100 AU from the Sun, so that most of the known TNOs are very faint ($R = 19$–22 mag) objects. As of today, more than 1200 such icy bodies have been detected beyond Neptune.

The primordial proto-planetary disk from which the planets emerged exhibits a complex dynamical history (Gladman et al. 2008) that involves gravitational stirring from the giant planets during the early ages of the solar system (Levison & Morbidelli 2003). Since TNOs are thought to be relatively

unaltered relics of this disk, they provide invaluable information about the history and evolution of the outer solar system.

Centaurs are a transient population between TNOs and Jupiter-family comets, orbiting in a region between Jupiter and Neptune. Currently, almost 400 of them are known and it is generally accepted that they share a common origin with the Kuiper belt objects. Since Centaurs are also typically brighter than the TNOs, they serve as a proxy from which it is possible to infer general properties on these more distant objects (Fernández et al. 2002).

Although a general picture of the TNO belt slowly emerges, many questions have remained unanswered. The size distribution of the TNOs remains uncertain, and knowledge of basic information about their surface properties, presence of atmosphere, bulk density, and internal structure is poor or even nonexistent. Yet these physical parameters are essential for assessing the present mass of the belt and retrieving its history. TNOs can be observed in visible bands to derive spectro-photometric properties and rotational light curves. They can also be detected in the IR (NASA/*Spitzer*, ESA/*Herschel* space telescopes), which provides an estimate of their size by combining their visible brightness and thermal emission. Results are model-dependent, however, and accuracies for their equivalent diameter of 10–20% at best can be obtained (Stansberry et al. 2008; Müller et al. 2009).

In contrast, stellar occultations are much more accurate, since kilometric accuracies can be achieved (see e.g. Sicardy et al. 2011; Ortiz et al. 2012) in the determination of their dimensions. This accuracy is much better than that obtained by other model-dependent, indirect methods. Not only sizes, but also shapes are derived from stellar occultations. Shapes are in turn related to density, elongation, and rotation to large TNOs (Braga-Ribas et al. 2013). This eventually yields a better estimate of size distribution and total mass of the material present beyond Neptune. Retrieving accurate sizes is also important as it allows us to derive accurate values for the albedos, an important parameter that constrains the nature of the surfaces (e.g. fresh bright ice vs. space-weathered dark, cometary-like material, see Elliot et al. 2010). Sizes also provide essential information on densities for TNOs with satellites (e.g. Pluto, Eris), since the masses can be derived from Kepler's laws. Densities, in turn, are an important parameter to constrain internal composition and structure of those bodies (e.g. rock/ice ratio). Another outstanding advantage of stellar occultations is the possibility of detecting very tenuous atmospheres around some of these bodies, down to surface pressure of a few nanobars, as reported for instance by Widemann et al. (2009), Sicardy et al. (2011), and Braga-Ribas et al. (2013). This is four orders of magnitudes lower than Pluto's surface pressure (about 10 μbar). Note that it is likely that the largest bodies (such as Eris, Haumea, or Makemake) are capable of retaining volatiles on their surfaces (Brown et al. 2011), which may lead to the presence of tenuous atmospheres that cannot be detected from other ground-based observations.

The fundamental difficulty associated with stellar occultations by TNOs is predicting them. The diameters of most TNOs are smaller than 50 milliarcseconds (mas) on the sky. This means that absolute astrometric accuracies of at least 50 mas on both the star position and the TNO ephemeris must be achieved to provide reasonable chances of detection. The most straightfoward approach to select possible occultations is by using the star positions listed in an astrometric catalogue, then carry out follow-up observations to improve the star position and pin down the shadow path after applying corrections to the TNO ephemeris.
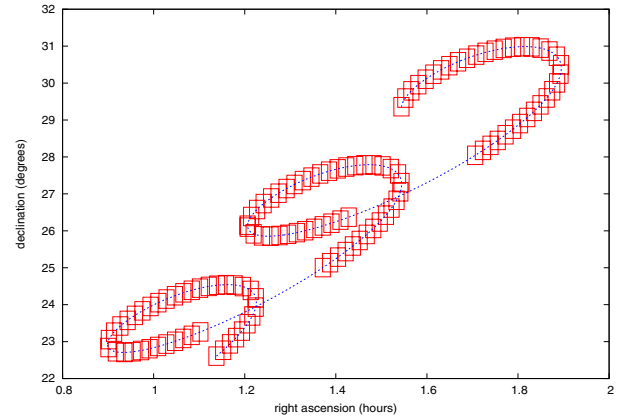
Fig. 1. Covering of the sky path of TNO (54598) Bienor from 2012 June 1 to 2014 Dec. 31. The blue (dashed) line represents the path of the TNO as seen by a ground-based observer. The region within the red (dotted) squares represent the area covered by the WFI mosaic. The uncovered segments of the path are those where the Sun-observer-target angle is smaller than 30°. The timeline starting point of the path is the bottom-left extremity of the blue (dashed) line. In this timeline, the frames corresponding to year 2013 start at RA about 0.9 h and end at RA about 1.2 h.

This paper is a continuation of the work presented by Assafin et al. (2010, 2012), to which we add occultation predictions and astrometric catalogues with the stellar contents from the sky paths of 5 Centaurs and 34 TNOs – for brevity, we refer to them simply as TNOs throughout. In Sect. 2, we present the observational design of this work and the observations themselves. In Sect. 3, we present the data reduction. Section 4 contains results and the respective analysis. In Sect. 5, we discuss the correction to the ephemerides. Section 6 presents the procedure for predicting the occultations. Comments and conclusions are given in Sect. 7. Throughout this paper, the notation $\alpha*$ stands for $\alpha \cdot \cos\delta$.

2. Observational design and respective observations – The ESO2p2/WFI TNO program

Observations designed to predict stellar occultations by TNOs frequently present two basic steps: first, the future sky path of a given TNO as seen by a ground-based observer is observed and an astrometric catalogue with positions and proper motions from the respective stellar content is produced; second, the TNO itself is observed so that we can determine a correction to its ephemeris.

Covering the sky path for a number of TNOs may be time-consuming from the observational point of view so that wide-field imagers, such as the Wide Field Imager (Baade et al. 1999) at the ESO/MPG 2.2 m Telescope (hereafter 2p2), are suitable for such a task. Figure 1 shows the observations to cover the sky path of (54598) Bienor. The clear overlap between images is necessary for the global reduction procedure (Sect. 3). Exposure times to all frames taken in the context to cover TNO sky paths were typically 30 s with the 2p2 standard broad-band *R* filter (filter number 844, λ_{central} = 651.725 nm, *FWHM* = 162.184 nm). The WFI is a mosaic of 8 (7′.5 × 15′) CCDs (largest dimension along declination), so that the mosaic covers an area of about 30′ × 30′ on the sky. Starting from the top leftmost CCD, they are numbered clockwise from 1 to 8.

Table 1. TNOs for which candidate stellar occultations for the period from 2012 Jun. 1st to 2014 Dec. 31st were predicted.

Target ID	Type	RA(J2000)Dec Easternmost	RA(J2000)Dec Westernmost	V	D (AU)	Diameter (km)	Source for diameter
(8405) Asbolus (also 1995 GO)	CEN	04:16 +37:05	03:19 +33:12	21.7	16.8	84	[1]
(24835) 1995 SM55	TNO	02:55 +30:48	02:34 +28:21	20.8	38.4	<704	[1]
(10199) Chariklo (also 1997 CU26)	CEN	17:41 −38:31	16:07 −39:52	18.2	14.5	248	[1]
(26375) 1999 DE9	TNO	12:07 −06:01	11:40 −02:40	20.6	37.3	461	[1]
(47171) 1999 TC36	TNO	02:11 +05:02	01:44 +02:13	19.8	30.6	393	[1]
(38628) Huya (also 2000 EB173)	TNO	15:53 −06:01	15:16 −04:07	19.3	28.6	458	[1]
(54598) Bienor (also 2000 QC243)	CEN	01:54 +30:30	00:54 +22:50	17.5	16.7	188	[1]
(55565) 2002 AW197	TNO	09:42 +00:48	09:25 +03:24	20.1	46.1	742	[1]
(55576) Amycus (also 2002 GB10)	CEN	17:50 −33:58	16:42 −34:08	20.2	18.1	101	[1]
(83982) Crantor (also 2002 GO9)	CEN	19:41 −19:46	18:36 −19:34	21.0	16.7	60	[1]
(119951) 2002 KX14	TNO	16:48 −22:39	16:28 −22:00	20.5	39.3	455	[1]
(307261) 2002 MS4	TNO	18:29 −07:42	18:13 −08:14	20.6	47.0	934	[1]
(84522) 2002 TC302	TNO	02:20 +25:49	02:05 +23:26	20.5	45.8	584	[1]
(55637) 2002 UX25	TNO	02:36 +10:12	02:18 +09:19	19.9	41.3	697	[1]
(55638) 2002 VE95	TNO	05:31 +08:43	04:59 +08:44	20.4	28.8	250	[1]
(119979) 2002 WC19	TNO	05:31 +19:00	05:12 +18:17	21.3	41.8	363	[2]
(120132) 2003 FY128	TNO	13:14 −15:59	12:50 −13:02	20.8	39.2	460	[1]
(174567) 2003 MW12	TNO	17:09 −02:41	17:00 −01:51	20.2	47.3	724	[2]
(120178) 2003 OP32	TNO	22:11 +02:29	21:52 +02:41	20.4	41.8	561	[2]
2003 UZ413	TNO	03:28 +06:23	03:11 +05:25	20.7	43.0	501	[2]
(84922) 2003 VS2	TNO	04:51 +33:44	04:24 +33:35	19.8	36.5	523	[1]
(90568) 2004 GV9	TNO	14:39 −25:59	14:12 −25:27	19.9	39.3	680	[1]
2004 NT33	TNO	21:23 +17:32	21:01 +16:00	20.5	38.5	457	[2]
(175113) 2004 PF115	TNO	22:46 −21:17	22:27 −22:51	20.8	41.5	468	[1]
(120347) Salacia	TNO	23:15 +20:40	22:58 +18:47	20.9	44.3	901	[1]
(120348) 2004 TY364	TNO	02:49 −09:18	02:29 −10:24	20.4	39.3	489	[2]
(144897) 2004 UX10	TNO	02:36 +05:54	02:16 +04:17	20.6	39.0	398	[1]
2005 CC79 (2011 FX62)	TNO	13:17 −27:28	12:14 −21:58	20.9	22.0	120	[2]
(303775) 2005 QU182	TNO	01:16 −05:38	01:02 −07:22	20.7	49.8	416	[1]
(145451) 2005 RM43	TNO	04:31 +12:06	04:08 +09:33	20.1	35.7	457	[2]
(145452) 2005 RN43	TNO	22:31 +00:57	22:12 −00:16	20.2	40.7	679	[1]
(145453) 2005 RR43	TNO	04:15 +08:43	03:56 +06:45	20.1	39.0	549	[2]
(202421) 2005 UQ513	TNO	00:37 +30:48	00:21 +29:09	20.4	48.5	724	[2]
2007 JH43	TNO	16:13 −21:05	15:52 −19:03	20.8	40.6	389	[2]
(278361) 2007 JJ43	TNO	16:24 −26:39	16:00 −26:33	20.1	41.4	575	[2]
(225088) 2007 OR10	TNO	22:23 −13:06	22:18 −13:50	21.5	86.7	1280	[1]
(229762) 2007 UK126	TNO	04:32 +00:00	04:14 −01:07	20.0	44.2	599	[1]
2008 OG19	TNO	20:33 −10:28	20:10 −11:11	20.7	38.6	417	[2]
2010 EK139	TNO	13:40 −34:54	13:12 −31:19	19.7	38.1	470	[1]

Notes. The classification TNO/Centaur is that adopted by the JPL. The easternmost and westernmost coordinates are an approximation of the limits within which the observations are found that covered the sky path of a given TNO, as seen from an earth-based observer, from 2012.5 to the end of 2014. The values given in the V column are just an indication of the apparent magnitudes for each object. The distances (D) are in astronomical units and refer to the JD given by Table 5. The references for the diameters are: [1] most recent value, by the time this paper was written, found in Johsnton's archive (http://www.johnstonsarchive.net/astro/tnodiam.html); [2] determined from the values of H and G as obtained from the physical parameter area contained in the ephemerides provided by the JPL, Horizons System.

The direct observations of the TNOs, aiming at an initial correction for their respective ephemerides and also to feed orbital computation procedures, were made on the basis of dither-offset-dither. This was performed so that the targets were always placed at some few arcminutes from the optical axis of the telescope. More specifically, a number of dithered images were taken with the target in the top right portion of CCD#7 and, after an offset of some few arcminutes, another number of dithered images were taken with the target now in the bottom-left portion of CCD#3. Exposure times were magnitude dependent and varied from 35 to 300 s, where 200 s was a typical figure. Again, the standard broad-band R filter was used. Table 1 lists all target names along

with some physical and observational parameters. These targets were chosen by taking into consideration their scientific interest, diameter size (larger diameters increase the occultation probability), position on the sky (proximity to the Galactic plane increases the occultation probability), and magnitude (too faint TNOs are out of reach for astrometry/photometry follow-up on small telescopes).

All the observations with the ESO/MPG 2p2+WFI were made in four consecutive runs (see Table 2), from 2011 to 2013, the seeing was in the range from 0''5 to 1''5 most of the time (≥60%) for all runs. As a general rule, the sky paths of the TNOs were covered during the first two runs (these paths were

Table 2. Observational runs.

Run ID	Start–End	Year
	(DD/MM–DD/MM)	
088.C-0434(A)	29/10–04/11	2011
089.C-0356(A)	24/06–30/06	2012
090.C-0118(A)	01/11–04/11	2012
091.C-0454(A)[a]	21/04–21/04	2013
091.C-0454(A)	04/05–07/05	2013

Notes. Runs carried out at the ESO-La Silla with the ESO/MPG 2p2+WFI. Runs start at noon of the first day and end at noon of the last day. [a] We obtained the second half of the night that started at noon of April 20 as a compensation time from GROND[1].

the most critical part of this work), whereas the direct observations of these bodies, aiming at obtaining an initial correction for their ephemerides, were made during the last two runs. Table 3 shows the number of mosaic frames used to cover the sky paths of the TNOs.

Each mosaic, after being corrected for overscan, bias and flatfield (see next section), occupies a space of 256MB. Therefore, from Table 3, one sees that about 550GB of images were processed for astrometry and photometry.

3. Data reduction

The data reduction followed the same steps as described in Assafin et al. (2010, 2012), based on IRAF (Tody 1993) plus esowfi (Jones, H. and Valdes 2000) and mscred (Valdes 1998) tasks (corrections for overscan, bias, flatfield) and PRAIA (Assafin et al. 2011) (field distortion pattern, astrometry and photometry). The few differences between the reduction made here with respect to the two previous works are enumerated below.

1. No bad-pixel mask was applied. These masks are insufficient to fix the astrometry of objects sampled on bad pixels but are good enough to cheat the eyes when examining an image to search for possible sources of a problematic point spread function (PSF) fitting.
2. All individual CCDs of each mosaic frame aiming at covering the sky paths of the TNOs had the UCAC4 (Zacharias et al. 2013) as reference for astrometry instead of the UCAC2 (Zacharias et al. 2004).
3. All individual CCD reduction of each mosaic aiming at the determination of positions for the TNOs had as reference for astrometry the catalogues obtained from the covering of the sky path of the respective TNOs. These catalogues include proper motion determination, as we explain below.

As in Assafin et al. (2010, 2012), a global solution provided the final set of positions to the stellar content in each yearly-covered sky path as well as to the direct observations of the TNOs. A global solution, by its nature, first determines a set of instrumental positions that must be then aligned to a given reference frame to provide the final set of positions. This instrumental system was determined through the results from the individual CCD reduction mentioned in item 3. Then, this instrumental system was aligned with the UCAC4. This is said to emphasise that all our positions are in the International Celestial Reference System (ICRS; Arias et al. 1995) as realised by the UCAC4.

---

[1] See http://www.mpe.mpg.de/~jcg/GROND/ for more details about GROND.

4. Results and analysis

Precise astrometric measurements were the basic aim to be attained from these observations. Magnitudes of all objects were also determined because these quantities play an important role when selecting among the final occultation predictions.

4.1. Sky paths

Exposure times of 30 s mentioned earlier are enough, under the typical sky of La Silla, to provide us with catalogues complete down to $R = 19.0$ (see Fig. 2) and with a limiting magnitude of $R = 21.0$. The expected nominal signal-to-noise ratio (S/N) to stars at $R = 19.0$ is about 65 in raw images under clear sky. Each object listed in Table 1 has, therefore, three such catalogues: one covering its sky path from 2012.5 to the end of 2012, another covering its sky path for the year 2013, and another covering its sky path for the year 2014. After 2014, astrometric releases of the GAIA (Perryman 2003) space mission are expected. All the positions from the mosaic catalogues are consistent with the primary reference catalogue UCAC4. To make it easier for the end user, we organised these catalogues according to the calendar year. Thus, if the user is observing the FOV of a TNO at a given date, he/she knows what catalogue to use by the calendar label because the stars contained in that FOV will be listed in that particular catalogue only.

These catalogues comprise a total of 12 456 565 entries and, in their original format, were used to search candidate stars to be occulted by the objects in Table 1. We also prepared a simplified version (that is, with fewer columns) of each catalogue[2] to serve as astrometric reference to the reduction of the individual CCDs from the mosaics with the direct observations of the TNOs[3]. An extract of such a catalogue, which we call WFI catalogue, is given in Table 4. Columns 8 and 9 of that table concern the uncertainties in proper motions and are always 99.999, indicating that they were not estimated. This is expected to change in the future so that we keep those columns to avoid changing formats in the programs that read these files.

From Cols. 4 and 5 in Table 5, we see that the median of the standard deviation of the measurements in right ascension and declination for the TNOs is 13 mas. If we consider the S/N of 65 mentioned above and a seeing of 1″2, a rough theoretical estimate for the precision of the centroid position of an stellar image would be 8 mas. This value should be compared with the value of 13 mas, which can also be understood as the internal precision of the measurements (the repeatability capability of the instrument measurements in position). This comparison supports an efficient PSF fitting and translation of CCD coordinates into equatorial coordinates.

Figure 3 shows the internal precisions in position as obtained from the reduction process of the images that covered the sky paths. In that figure, where the images were integrated for 30 s, we notice that the precisions of faint ($R \gtrsim 19.0$) objects are significantly poorer than the value of 13 mas of the internal precision of the TNO's positions. The S/N of 65 associated to integrations of 30 s is a theoretical value that in practice was not achieved. To image the sky paths, this integration time was kept regardless of the observational conditions. On the other hand, the images aimed at the astrometry of the TNOs were acquired

---

[2] Available at the CDS and also at http://funk.on.br/camargo/WFIBC/ and ftp://ftp.imcce.fr/pub/catalogs/WFIBC/
[3] Of course, these catalogues can be used as an astrometric reference to any astronomical image that contains the covered sky region.

Table 3. Characteristics of the catalogues from the observations that covered the sky paths of TNOs.

Target ID	#Frames	Complete R	#Entries	$\sigma_{\alpha*}$ σ_{δ} (mas)	Proper motions (%) UC4	2M	UB1	$f0$ (%)	Predictions 2012.5	2013	2014
(8405) Asbolus	103	18.5	218 863	50 53	15.7	39.3	31.7	97.7	34	48	40
(24835) 1995 SM55	52	19.0	54 357	51 53	16.2	37.1	28.5	96.4	7	7	8
(10199) Chariklo	131	19.0	2 986 471	56 56	6.6	34.4	8.7	96.2	415	768	689
(26375) 1999 DE9	39	19.0	24 340	49 49	13.9	32.9	32.9	96.2	1	3	7
(47171) 1999 TC36	58	20.0	43 333	49 48	9.2	22.4	27.9	91.4	4	8	4
(38628) Huya	67	19.5	97 374	49 48	11.1	26.0	32.3	96.1	11	12	10
(54598) Bienor	122	19.0	96 379	49 51	16.8	32.5	32.3	96.0	27	17	21
(55565) 2002 AW197	40	18.0	19 381	52 52	21.7	38.8	21.1	96.3	6	3	3
(55576) Amycus	98	18.5	2 704 031	56 55	6.1	28.6	9.7	93.7	655	601	540
(83982) Crantor	87	19.5	2 952 104	56 56	4.9	12.1	14.4	92.3	1240	622	257
(119951) 2002 KX14	21	19.0	149 784	54 53	6.8	31.9	29.6	96.7	21	48	40
(307261) 2002 MS4	42	19.0	887 401	58 58	1.7	45.7	1.5	95.0	55	130	125
(84522) 2002 TC302	44	19.5	48 318	48 48	12.1	25.1	25.0	95.2	1	8	7
(55637) 2002 UX25	43	19.5	26 332	49 48	13.0	30.9	30.9	93.5	0	5	5
(55638) 2002 VE95	67	19.5	174 945	51 49	12.8	27.2	31.9	97.4	9	19	17
(119979) 2002 WC19	27	19.0	103 449	51 51	13.3	34.1	29.8	98.1	16	27	12
(120132) 2003 FY128	36	19.0	38 338	49 49	12.1	24.9	27.0	95.5	5	4	8
(174567) 2003 MW12	46	18.5	141 589	50 50	10.3	31.2	39.3	97.2	15	17	20
(120178) 2003 OP32	50	19.5	59 373	49 48	12.7	27.6	39.7	96.4	4	10	6
2003 UZ413	46	19.5	28 386	48 47	13.0	31.9	25.0	94.1	3	2	4
(84922) 2003 VS2	52	19.0	154 542	53 55	11.0	45.2	23.5	97.4	8	21	26
(90568) 2004 GV9	45	19.0	91 313	48 48	11.3	27.5	36.4	97.2	5	10	9
2004 NT33	73	19.0	233 652	52 51	13.0	25.4	35.7	98.1	20	34	35
(175113) 2004 PF115	47	19.5	39 361	50 47	11.4	25.8	41.9	94.7	3	4	4
(120347) Salacia	53	19.0	53 301	49 49	14.2	31.5	30.7	96.0	4	2	5
(120348) 2004 TY364	60	20.0	37 313	50 50	11.2	27.5	31.8	91.1	9	6	6
(144897) 2004 UX10	47	19.0	25 330	50 50	13.8	32.2	27.9	92.4	4	2	5
2005 CC79 (2011 FX62)	91	18.5	100 177	49 48	13.2	32.3	34.7	96.5	9	29	23
(303775) 2005 QU182	39	19.5	19 736	51 49	11.1	29.2	34.5	91.2	2	3	4
(145451) 2005 RM43	40	18.5	35 313	50 49	15.8	43.4	19.4	96.4	5	4	5
(145452) 2005 RN43	44	19.5	43 316	49 47	12.1	28.9	32.9	96.2	4	6	6
(145453) 2005 RR43	50	19.5	42 344	48 48	13.3	33.5	28.7	95.9	4	6	5
(202421) 2005 UQ513	49	19.0	47 355	50 51	18.1	31.5	32.9	96.3	2	4	6
2007 JH43	24	19.0	99 340	50 50	10.5	26.9	34.1	97.0	12	24	25
(278361) 2007 JJ43	34	19.0	231 336	50 49	7.5	28.5	26.7	97.5	15	38	27
(225088) 2007 OR10	15	19.5	16 362	49 50	12.4	26.4	38.7	96.9	6	4	3
(229762) 2007 UK126	51	20.0	55 328	51 49	11.8	29.1	27.0	95.4	2	6	3
2008 OG19	45	19.0	144 725	51 51	9.7	24.6	38.9	97.6	24	36	20
2010 EK139	60	19.0	126 373	50 50	12.1	29.9	37.0	97.1	12	17	9

Notes. Column 1: TNO ID; Col. 2: total number of WFI frames used to cover the sky path of the respective TNO from 2012.5 to the end of 2014; Col. 3: magnitude completeness; Col. 4: total number of entries for all three catalogues with positions and proper motions (WFI catalogues, see text); Cols. 5 and 6: standard deviation of the offsets (observed minus catalogue position) in right ascension and declination, respectively, for the UCAC4 stars; Cols. 7 to 9: per cent of stars whose proper motions came directly from the UCAC4 or from a combination between the observed (WFI) position and either 2MASS or USNO-B1; Col. 10: per cent of stars in the positions and proper motions catalogue that have $f0$ for quality astrometry. Flags range from 0 ($f0$: good astrometry) to 5 ($f5$: position derived from one measurement only). The lower the flag number, the more reliable the position (see Assafin et al. 2010, 2012 for further details); Cols. 11 to 13: number of predicted events per year. No selection was made in this counting so that, for instance, occultations occurring during daylight were also considered.

to ensure that these faint objects had a high enough S/N for good astrometry (the typical integration time was 200 s). In addition, the observational strategy kept these objects in a constrained area of the mosaic, close to the optical axis of the instrument, so that the effects of an imperfect corretion of the field distortion pattern are weaker. This was certainly not the case for the images acquired for the astrometry of the sky paths.

From Cols. 5 and 6 in Table 3, we notice that the standard deviations for the measured positions of the reference stars is typically 50 mas, which is higher than those presented in Fig. 3. This

is expected because the uncertainties in Fig. 3 reflect the internal precision of the measurements, while Cols. 5 and 6 of Table 3 basically reflect the uncertainties of the UCAC4[4] stars at the WFI observation epoch. Overall, 50 mas is the highest value that represents the uncertainties of the measurements presented here.

---

[4] The problem with the data related to some high proper motions in UCAC4, as pointed out in http://www.usno.navy.mil/USNO/astrometry/optical-IR-prod/ucac, is known and the script to correct for it was properly applied.
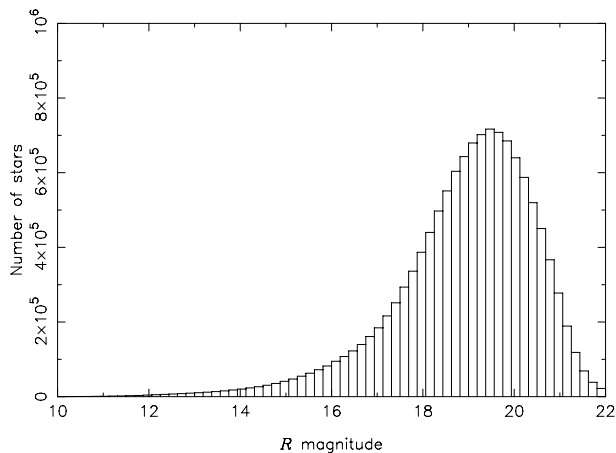
Fig. 2. Histogram of the magnitudes for all objects in the observations of the sky paths of the TNOs, in bins of 0.19 mag.

In addition, this value is associated to the stars that realise, in this work, the adopted celestial frame (ICRS). Therefore, it is safe to adopt that value as representative of the precision of the observed positions of TNOs and of stars contained in the catalogues that are derived from the observations of the sky paths. All the observational data in Table 3 come from the ESO/MPG 2p2+WFI.

A clear exception to the adoption of 50 mas to the precision in position is the Centaur (8405) Asbolus. It is the faintest solar system object in Table 1, and the dispersion of the measurements (see Cols. 4 and 5 of Table 5) is an indication that a lower precision in position should be associated to this object. Our suggestion is to use the $\sigma_{\alpha*}$ and σ_δ values from Table 5 in this case.

4.2. Observation of the TNOs

Most ephemerides for the TNOs, for instance, those available from the JPL HORIZONS service, are frequently upgraded to better represent the real orbit of these bodies. But the accuracies of these ephemerides are still not good enough to be used in the work of occultation prediction. To perform these corrections and also redetermine the orbits, the observation of these bodies are of the utmost importance. Table 5 summarizes the main results from these observations, for which the WFI catalogues were fully exploited. All the observational data in Table 5 come from the ESO/MPG 2p2+WFI.

5. Correction for the ephemerides

We used the ephemerides obtained from the JPL HORIZONS telnet service as primary source for the positions of TNOs. The required refined knowledge of these positions may be obtained by either a correction of the respective ephemerides, or by redetermining the TNO orbits. The correction may be given in the form of a (time-dependent) single offset as obtained from the difference between observed and ephemeris positions (offset method). The redetermination of TNO orbit (ephemeris method) depends on the availability of a number of observed positions and of a code for the numerical integration of the equations of motion. We used the code Numerical Integration of the Motion of an Asteroid (NIMA – see next subsection) to update and refine the predictions presented here.

Redetermining the ephemeris allows us to propagate the correction to future dates (a few years ahead, for instance), but

requires the availability of additional observations spread over a time span of some years – from the Minor Planet Center (MPC), for instance – as well as continuous observational work.

Experience shows that the offset method is thoroughly useful as a starting point to determine the predicitons. Indeed, we note that

1. Frequently, the observed and ephemeris positions of a given TNO are offset by high values (hundreds of milliarcseconds). Therefore, although this offset is time dependent and not accurate enough to precisely predict a future occultation (one year after the acquisition of the observation from which the offset was determined, for instance), we are definitely aware that this is possible, so that we can proceed with the necessary refinements in due course. This scenario is by far better than making no predictions and taking the risk of losing an occultation.

2. Frequently, using different sets of observations of a TNO made close in time results in the application of very different offsets on the respective ephemeris. An orbit determination from these sets of observations would be inaccurate, which means that we would have to wait for more observational data.

In this context, all predictions in this work were made with the offset method; offsets in the sense observed minus ephemeris positions for all TNOs are listed in Table 5.

The ephemeris method, however, yields more reliable TNO positions (see also Fraser et al. 2013) at dates far from those of the observed positions (compare the uncertainties in the two panels in Fig. 4). In this context we performed updates and refinements of our predictions by considering the ephemeris method as frequently as possible. Of course, refinements on the position of the candidate star to be occulted were performed constantly.

Figure 4 shows a comparison between results from NIMA and JPL ephemerides for the Centaur (10199) Chariklo. On the leftmost vertical lines (both panels) of that figure are found the offsets (solid circles) in the sense observation minus JPL, where the observations were made at the Pico dos Dias Observatory (OPD)/LNA in 2011. On the two next vertical lines (both panels) are found the offsets in the sense observation minus JPL, where observations were made during two close nights at the ESO-La Silla (last run, see Table 2). The offsets as determined from the June 2013 occultation (see Fig. 5) were then assumed to be on the intersection of the rightmost line with the blue (grey) and black thick lines shown in the right panel. The uncertainty of the differences between NIMA and JPL is much smaller in the right panel. This feature helps us to predict stellar occultations more accurately and highlights the need of frequent observations of TNOs to improve their ephemerides.

5.1. Ephemeris determination

The ephemeris determination makes use of the code NIMA. The dynamical model takes into account the perturbations of the eight planets, and we considered the EMB instead of Earth and Moon. The positions of the planets (or the barycenter of the system where the planets are) are provided by JPL planetary ephemerides DE421 (Folkner et al. 2009). Adding the perturbations of the three main asteroids (Ceres, Pallas, and Vesta) has no consequence on the motion of Centaurs or TNOs, because of their masses and the distance between these objects. The equations of motion were numerically integrated with a Gauss-Radau method (Everhart 1985) as well as the variational equations used to fit the dynamical model. The fitting process

Table 4. Extract of the WFI catalogue for the Centaur (10199) Chariklo.

RA (ICRS)	DEC	$E_{\alpha*}$	E_δ	JD (UTC)	$\mu_{\alpha*}$	μ_δ	$E_{\mu_{\alpha*}}$	E_{μ_δ}	R	E_R
		(arcsec)			(arcsec/year)		(arcsec/year)			
16 56 06.4863	−40 31 30.202	0.021	0.021	2 456 104.77607956	0.017	−0.010	99.999	99.999	12.302	0.615
16 55 42.3301	−40 31 33.053	0.022	0.022	2 456 104.77749181	−0.008	−0.012	99.999	99.999	19.078	0.615
16 55 59.9121	−40 31 32.044	0.022	0.023	2 456 104.77607956	−0.009	−0.010	99.999	99.999	18.778	0.615
16 55 43.9452	−40 31 30.627	0.021	0.021	2 456 104.77749181	−0.007	−0.005	99.999	99.999	15.667	0.615
16 55 48.9368	−40 31 31.219	0.023	0.023	2 456 104.77607956	−0.008	−0.014	99.999	99.999	17.937	0.615
16 55 45.8457	−40 31 31.017	0.033	0.034	2 456 104.77607956	−0.003	−0.029	99.999	99.999	19.013	0.615
16 56 03.4612	−40 31 29.732	0.020	0.020	2 456 104.77607956	−0.001	0.004	99.999	99.999	17.879	0.615
16 55 46.4453	−40 31 28.596	0.022	0.022	2 456 104.77607956	−0.012	−0.008	99.999	99.999	17.550	0.615
16 56 04.6101	−40 31 26.393	0.021	0.021	2 456 104.77607956	−0.022	0.003	99.999	99.999	13.216	0.615
16 55 35.8488	−40 31 25.505	0.021	0.021	2 456 104.77749181	−0.003	−0.004	99.999	99.999	17.576	0.615

Notes. Extract of one ((10199) Chariklo) of the WFI catalogues that were used in the reduction of the individual CCDs of the WFI that contained the observations of the TNOs. They are narrower (fewer columns) versions of the positions and proper motion catalogues that were used to determine the predictions. The uncertainties in position ($E_{\alpha*}$ and E_δ) are a combination of the fitting uncertainty and the standard error from the variance-covariance matrix of the least-squares reduction that translated each (x, y) coordinate on the WFI CCDs into right ascension and declination in the ICRS. The Julian date is the origin for proper motion displacement. Magnitudes (R) are the observed ones, with the respective errors (E_R).
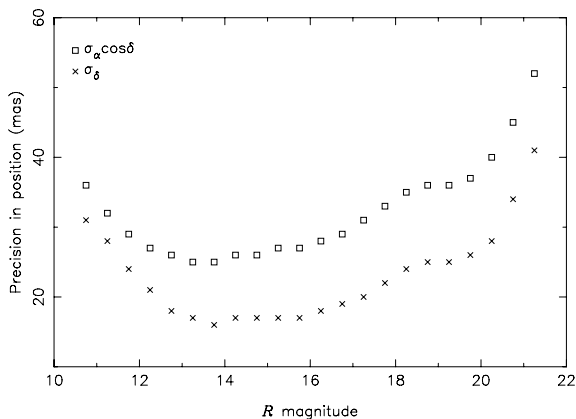

Fig. 3. Internal precisions in right ascension and declination to all stars from the observations of the sky paths. These precisions were determined as follows: standard deviations were grouped in bins of 0.5 mag and then the mean value was taken. The standard deviations of each star are obtained from the global reduction technique (see Sect. 3) by considering each position of the star and the resulting mean position. Each symbol represents the average of at least 1000 measurements.

consists of determining the state vector of the asteroid that minimizes the difference between computed and observed positions, as explained in Desmars et al. (2009). The observations come from the Minor Planet Center[5] or the AstDyS[6] database, and from other databases or observatories. The precision of observations can be taken into account in the fitting process by giving a weight to each observation. The AstDyS database provides an estimated accuracy of each observation that is used in our process. Finally, the dynamical model fitted on observations provides the asteroid ephemeris, whose accuracy can be estimated from the propagation of the covariance matrix (see, for instance, Desmars et al. 2013).

6. Occultation predictions

The prediction of the occultation is obtained by crossing the stellar catalogues of positions and proper motions presented before

with a given ephemeris. Again, the same procedures as reported by Assafin et al. (2010, 2012) were used, therefore we only briefly describe them here.

In our catalogues of positions and proper motions (one per year per TNO), positions (see details in Table 3) are obtained from the stellar content in the observations that covered the sky paths. Proper motions are determined as follows:

1. If the star is in the UCAC4, take the proper motion from there.
2. If the star is not in the UCAC4, search for it in the 2MASS point source catalogue (Skrutskie et al. 2006). If found, determine its the proper motion.
3. If the star is found neither in UCAC4 nor in 2MASS, search for it in the USNO-B1.0 (Monet et al. 2003). If found, determine its proper motion. If not, no proper motion is determined.

Whatever the source for the ephemeris, either JPL (offset method correction) or NIMA, we use the geometry space information system SPICE (Acton 1996) tools to read them and the SOFA[7] and NOVAS[8] software to perform, when necessary, transformations involving earth orientation parameters. With this, a one-minute step position ephemeris is generated for each TNO and is then compared with the stellar catalogue of positions and proper motions. The final output is an ascii table, as shown by Table 6, with the necessary information to produce occultation maps (see Fig. 5).

We emphasize that all the results are made publicly available: occultation maps[9], occultation tables (example given by Table 6) can be obtained from the CDS, and the WFI catalogues can be obtained from the sites mentioned earlier in the text. All updates and refinements concerning the predictions are reported.

---

[5] http://www.minorplanetcenter.net/
[6] http://hamilton.dm.unipi.it/astdys
[7] http://www.iausofa.org/
[8] http://aa.usno.navy.mil/software/novas/novas_info.php
[9] Example given by Fig. 5 can be obtained from the link http://www.lesia.obspm.fr/perso/bruno-sicardy/

Table 5. Observed minus ephemeris positions for the TNOs in Table 1.

Target ID	$\Delta\alpha*$	$\Delta\delta$	$\sigma_{\alpha*}$	σ_δ	Mean	#Ref. stars	#Used	Ephemeris
	(mas)		(mas)		JD (UCT)	per frame	measur.	version
(8405) Asbolus	+228	+154	77	108	2 456 235.7	349	4	JPL#41
(24835) 1995 SM55	+357	+158	20	45	2 456 233.7	254	10	JPL#10
(10199) Chariklo	−264	+118	12	6	2 456 412.3	840	15	JPL#20
(26375) 1999 DE9	−501	+065	20	29	2 456 418.5	124	28	JPL#15
(47171) 1999 TC36	+623	−082	8	12	2 456 235.6	104	4	JPL#8
(38628) Huya	−511	−035	8	39	2 456 415.3	186	20	JPL#16
(54598) Bienor	+118	−055	28	36	2 456 235.6	197	4	JPL#27
(55565) 2002 AW197	+055	+171	20	25	2 456 419.0	138	15	JPL#10
(55576) Amycus	−605	+175	13	67	2 456 411.2	369	13	JPL#3
(83982) Crantor	−877	−080	10	2	2 456 418.9	1132	7	JPL#15
(119951) 2002 KX14	−107	−076	28	37	2 456 411.2	467	15	JPL#9
(307261) 2002 MS4	−331	−042	23	10	2 456 419.3	263	16	JPL#10
(84522) 2002 TC302	−029	−158	36	11	2 456 235.7	208	4	JPL#10
(55637) 2002 UX25	+159	−001	13	8	2 456 234.7	131	10	JPL#14
(55638) 2002 VE95	+042	+016	15	6	2 456 235.7	520	4	JPL#6
(119979) 2002 WC19	+527	−322	14	8	2 456 235.7	601	4	MP245016
(120132) 2003 FY128	−195	+018	12	13	2 456 418.7	168	23	JPL#6
(174567) 2003 MW12	+184	−452	14	16	2 456 411.8	465	16	MP186748
(120178) 2003 OP32	−083	−162	12	7	2 456 234.6	282	9	JPL#9
2003 UZ413	−362	−385	18	9	2 456 233.8	133	9	MP227411
(84922) 2003 VS2	−17	−129	12	14	2 456 235.7	392	4	JPL#15
(90568) 2004 GV9	+116	+077	3	15	2 456 418.2	314	12	JPL#5
2004 NT33	−440	−687	11	18	2 456 419.9	519	8	MP224606
(175113) 2004 PF115	−439	−211	13	9	2 456 233.7	142	10	MP226985
(120347) Salacia	+610	−227	5	11	2 456 233.6	228	9	JPL#9
(120348) 2004 TY364	−793	−258	11	7	2 456 233.8	85	10	JPL#2
(144897) 2004 UX10	+1488	+097	17	11	2 456 234.8	109	7	MP157314
2005 CC79 (2011 FX62)	−817	−199	9	19	2 456 418.4	201	21	MP202199
(303775) 2005 QU182	+1048	+237	14	3	2 456 234.7	85	6	MP208925
(145451) 2005 RM43	+104	−059	24	13	2 456 234.8	216	9	MP226879
(145452) 2005 RN43	+134	−022	7	6	2 456 233.6	195	9	MP241106
(145453) 2005 RR43	−175	−103	7	14	2 456 234.8	184	9	MP186683
(202421) 2005 UQ513	+757	+237	39	26	2 456 235.6	239	5	MP241355
2007 JH43	+526	−773	17	9	2 456 418.5	523	32	MP224657
(278361) 2007 JJ43	−821	−559	9	5	2 456 418.4	706	16	MP197647
(225088) 2007 OR10	−061	−362	17	21	2 456 235.0	131	10	MP211433
(229762) 2007 UK126	−038	−440	12	10	2 456 233.8	177	10	MP186835
2008 OG19	−065	+506	11	16	2 456 419.9	377	7	MP235388
2010 EK139	−171	−604	19	12	2 456 418.2	336	16	MP206188

Notes. Column 1: TNO ID; Cols. 2 and 3: offsets in the sense observed minus ephemeris positions for the respective TNO. These values result from a global reduction procedure; Cols. 4 and 5: internal precision of the offsets; Col. 6: Julian date; Col. 7: number of used references (UCAC4) stars; Col. 8: number of measurements used to estimate the figures in Cols. 2 to 5; Col. 9: TNO respective ephemeris version. All the ephemerides were taken from the HORIZONS JPL telnet service and were read with NASA's SPICE tools.

7. Comments and conclusions

We have presented stellar occultation predictions to selected 5 Centaurs and 34 TNOs from 2012.5 to the end of 2014. The whole observational data were obtained during four consecutive runs at La Silla – from October 2011 to May 2013 (see Table 2) – with the ESO 2p2 equipped with the Wide Field Imager. As of 2015, astrometric results from GAIA will provide stellar catalogues with positions and proper motions with unprecedented (microarcsecond) precision so that only refinements on the occulting bodies' ephemerides will be necessary (note in Fig. 4 the amplitudes of the differences between the NIMA and JPL ephemerides for (10199) Chariklo).

Sky paths covering regions of the sky where the TNO has already passed are still useful if one wants to refer to the respective past occultation and obtain a better astrometry of the occulting object. In addition, images associated to either past or future paths of a given TNO are, due to their limiting magnitudes, useful to investigate background stars that were or will be connected with the occulting body. The WFI catalogues, derived from the observations of the sky paths, provide useful catalogues that can serve as astrometric reference for astronomical images containing the covered regions.

At the time of the writing, the observations related to a precisely predicted occultation by the Centaur (10199) Chariklo (Fig. 5) were succesfully made and the respective results will
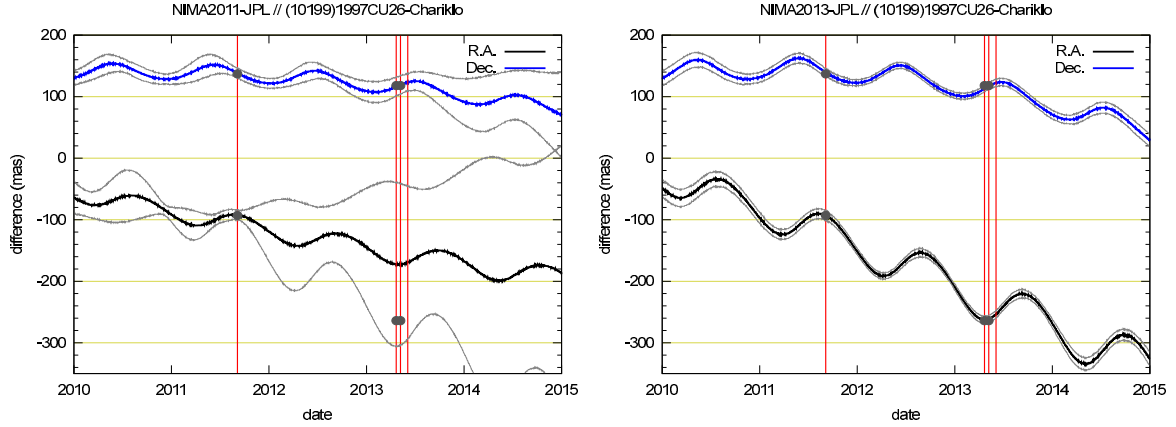
Fig. 4. Differences in position in the sense NIMA minus JPL ephemeris (same ephemeris version as that given in Table 5) for Centaur (10199) Chariklo. *Left panel*: differences in right ascension (black thick line) and declination (grey/blue thick line), where NIMA used observational data from the MPC and from the OPD. The thin grey lines show the 1-σ uncertainty of the differences. *Right panel*: differences in right ascension (black thick line) and declination (grey/blue thick line), where NIMA used observational data from the MPC and from the OPD and ESO.

Table 6. Extract of a prediction table.

d m Year	h m s	RA	(ICRS) Dec	C/A	P/A	v	D	$R*$	$J*$	$H*$	$K*$	λ	LST	$\Delta e_{\alpha*}$	Δe_δ	pm	ct	f	$E_{\alpha*}$	E_δ	$\mu_{\alpha*}$	μ_δ
03 06 2013	06:27:04.	16 56 6.4876	−40 31 30.211	0.171	10.69	−21.65	13.58	12.4	8.8	7.7	7.3	265.	00:08	−264.0	118.0	ok	uc	0	9999	9999	17	−10
03 06 2013	09:12:02.	16 56 4.6083	−40 31 26.390	0.400	10.74	−21.66	13.58	13.3	12.0	11.7	11.7	224.	00:08	−264.0	118.0	ok	uc	0	9999	9999	−22	3
04 06 2013	21:23:31.	16 55 39.9220	−40 30 30.263	0.640	191.40	−21.72	13.57	19.2	15.9	14.7	14.8	40.	00:01	−264.0	118.0	no	2m	0	73	23	9999	9999
05 06 2013	06:56:33.	16 55 33.3901	−40 30 15.737	0.043	191.55	−21.74	13.57	18.3	15.3	14.6	14.2	256.	00:00	−264.0	118.0	ok	2m	0	36	29	−6	−1
05 06 2013	09:54:16.	16 55 31.3683	−40 30 10.951	0.093	191.62	−21.74	13.57	18.6	14.1	13.0	12.5	211.	23:59	−264.0	118.0	ok	2m	0	39	17	−9	−1
05 06 2013	14:45:21.	16 55 28.0486	−40 30 3.531	0.301	11.72	−21.75	13.57	19.6	15.4	13.5	13.1	138.	23:58	−264.0	118.0	no	2m	0	131	146	9999	9999
05 06 2013	16:17:13.	16 55 27.0094	−40 30 0.709	0.054	191.73	−21.75	13.57	17.3	15.1	14.5	14.2	115.	23:58	−264.0	118.0	ok	2m	0	26	19	−16	6
06 06 2013	01:13:29.	16 55 20.9095	−40 29 45.986	0.204	191.90	−21.77	13.57	19.8	15.7	15.2	14.2	341.	23:56	−264.0	118.0	ok	2m	1	9999	9999	−23	−2
06 06 2013	02:28:45.	16 55 20.0596	−40 29 43.563	0.573	191.93	−21.77	13.57	19.3	15.4	14.7	14.3	322.	23:56	−264.0	118.0	ok	2m	0	45	24	−13	−23
06 06 2013	07:57:53.	16 55 16.3135	−40 29 34.562	0.508	192.03	−21.77	13.57	18.1	14.9	14.3	14.1	239.	23:55	−264.0	118.0	ok	2m	0	26	9	2	−1

Notes. Occultation table: day of the year and UTC time of the prediction; right ascension and declination of the occulted star – in the original table, these coordinates are immediately followed by the geocentric astrometric equatorial coordinates (corrected for the offset or ephemeris method), not presented here, of the occulting body; C/A: the geocentric closest approach, in arcseconds; P/A: the planet position angle with respect to the occulted star at C/A, in degrees; velocity in plane of sky, in km s^{-1}: positive = prograde, negative = retrograde; D: planet range to Earth, in AU; $R*$, $J*$, $H*$, $K*$: normalized magnitudes to a common shadow velocity of 20 km s^{-1} by the relationship Mag* = Mag$_{\text{actual}}$ + 2.5 × log 10($\frac{\text{velocity}}{20 \text{ km s}^{-1}}$). A value of 50.0 means that the star is not in the 2MASS; λ: east longitude of subplanet point in degrees, positive towards east; LST: UT + λ: local solar time at subplanet point, hh:mm; $\Delta e_{\alpha*}$ and Δe_δ: offset in mas applied to the ephemeris right ascension and declination, respectively; pm: ok = proper motion applied, no = no proper motion applied; catalogue cross-identification (ct) = uc (UCAC2), 2 m (2MASS), fs (field star); f = multiplicity flag (see Table 3); $E_{\alpha*}$ and E_δ: uncertainties (mas) in right ascension and declination. A value of 9999 means that there was no estimation of the respective uncertainty; $\mu_{\alpha*}$ and μ_δ: proper motions in right ascension and declination, respectively (mas/year).
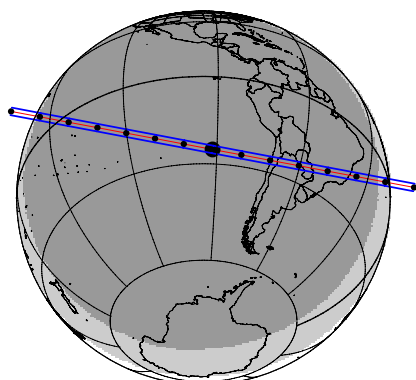
appear in a paper by Braga-Ribas et al. (2013, in prep.). The occultation by (119951) 2002 KX14 on 26 Apr. 2012 (observed in La Palma, Spain) was not predicted because the occultation occurred before our observations to cover its future path on the sky (second run at La Silla, see Table 2). However, now that the path is covered, we noticed that it would have been correctly predicted. Confirmation of past occultations is a valid test for our procedures and calculations to predict occultations.

As discussed by Assafin et al. (2010, 2012) a tentative way of estimating the probability of success of an occultation prediction is to consider the ratio of the apparent diameter of the TNO to its ephemeris offset uncertainty (see Table 5). Due to the use of the positions and proper motions catalogue in the reduction of the individual CCDs from the direct observations of the TNOs, the use of the uncertainty data on Table 5 would overestimate that probability. Instead, the use of the uncertainty from the ephemeris redetermination, when available, would be more suitable. Otherwise, the value of 50 mas should be used.

The reduction procedure follows the same method applied in Assafin et al. (2010) and Assafin et al. (2012). The most relevant differences are 1. use of the UCAC4 catalogue instead of UCAC2 and 2. the use of the catalogues with stellar positions and proper motions as derived from the observations of the sky paths (see Sect. 4) to reduce the observations of the TNOs and, consequently, obtain the offsets. This last feature, in particular, provides a better consistency between the positions of the occulting and occulted bodies.

General characteristics concerning the astrometry for both sky paths and solar system objects are provided in Tables 3 and 5. From the first of these tables, a mean standard deviation of 50 mas is obtained from the differences between observed and catalogue positions of reference (UCAC4) stars on both equatorial coordinates. These values can be taken as the mean accuracy of all the observed positions. From the latter of these tables, we obtained the offsets in position of each observed solar system target with respect to its respective ephemeris. These

−Chariklo− dots each 1000km or 46.19s <> offsets (mas) −264.0 118.0

d m year	h:m:s UT	ra___dec___J2000_candidate	C/A	P/A	vel	Delta	R*	K*	long
03 06 2013	06 27 04.0	16 56 06.4876 −40 31 30.211	0.171	10.69	−21.65	13.58	12.4	7.3	−95

Credits: Rio Team & B. Sicardy

Fig. 5. Occultation map for (10199) Chariklo. Compare the information given in caption with the first entry of Table 6.

offsets were used to make a first determination of the predictions and also to help us in the organization of future events. However, new orbit determinations through NIMA were used, whenever possible, to update forthcoming events[10].

The catalogues with stellar positions and proper motions are complete down to $R = 19$. Although this magnitude value may sound out of reach for many small telescopes, it is important to remember that the electron-multiplying technology, available on many cameras, makes occultation events involving faint stars ($R = 16$–17) detectable by 40 cm-class telescopes, for instance.

References

Acton, C. H. 1996, Planet. Space Sci., 44, 65
Arias, E. F., Charlot, P., Feissel, M., & Lestrade, J. 1995, A&A, 303, 604
Assafin, M., Camargo, J. I. B., Vieira-Martins, R., et al. 2010, A&A, 515, A32
Assafin, M., Vieira-Martins, R., Camargo, J. I. B., et al. 2011, in Gaia FUN-SSO workshop Proc., eds. P. Tanga, & W. Thuillot, 85
Assafin, M., Camargo, J. I. B., Vieira-Martins, R., et al. 2012, A&A, 541, A142
Baade, D., Meisenheimer, K., Iwert, O., et al. 1999, The Messenger, 95, 15
Braga-Ribas, F., Sicardy, B., Ortiz, J. L., et al. 2013, ApJ, 773, 26
Brown, M. E., Burgasser, A. J., & Fraser, W. C. 2011, ApJ, 738, L26
Desmars, J., Arlot, S., Arlot, J.-E., Lainey, V., & Vienne, A. 2009, A&A, 499, 321
Desmars, J., Bancelin, D., Hestroffer, D., & Thuillot, W. 2013, A&A, 554, A32
Elliot, J. L., Person, M. J., Zuluaga, C. A., et al. 2010, Nature, 465, 897
Everhart, E. 1985, in Dynamics of Comets: Their Origin and Evolution, eds. A. Carusi, & B. Giovanni (Dordrecht: Reidel), Proc. IAU Coll., 83, Astrophys. Space Sci. Lib., 115, 185
Fernández, Y. R., Jewitt, D. C., & Sheppard, S. S. 2002, AJ, 123, 1050
Folkner, W., Williams, J., & Boggs, D. 2009, JPL IPN Progress Reports, 42, 1
http://ipnpr.jpl.nasa.gov/index.cfm
Fraser, W. C., Gwyn, S., Trujillo, C., et al. 2013, PASP, 125, 1000
Gladman, B., Marsden, B. G., & Vanlaerhoven, C. 2008, in The solar system beyond Neptune, eds. M. A. Barucci, H. Boehnhardt, D. P. Cruikshank, A. Morbidelli, & R. Dotson (Tucson: University of Arizona Press), 43
Jones, H., & Valdes, F. G. 2000, Handling ESO WFI Data With IRAF
Levison, H. F., & Morbidelli, A. 2003, Nature, 426, 419
Monet, D. G., Levine, S. E., Canzian, B., et al. 2003, AJ, 125, 984
Müller, T. G., Lellouch, E., Böhnhardt, H., et al. 2009, Earth Moon and Planets, 105, 209
Ortiz, J. L., Sicardy, B., Braga-Ribas, F., et al. 2012, Nature, 491, 566
Perryman, M. A. C. 2003, in Gaia Spectroscopy: Science and Technology, ed. U. Munari, ASP Conf. Ser., 298, 3
Sicardy, B., Ortiz, J. L., Assafin, M., et al. 2011, Nature, 478, 493
Skrutskie, M. F., Cutri, R. M., Stiening, R., et al. 2006, AJ, 131, 1163
Stansberry, J., Grundy, W., Brown, M., et al. 2008, in The solar system beyond Neptune, eds. M. A. Barucci, H. Boehnhardt, D. P. Cruikshank, A. Morbidelli, & R. Dotson (Tucson: University of Arizona Press), 161
Tody, D. 1993, in Astronomical Data Analysis Software and Systems II, eds. R. J. Hanisch, R. J. V. Brissenden, & J. Barnes, ASP Conf. Ser., 52, 173
Valdes, F. G. 1998, in Astronomical Data Analysis Software and Systems VII, eds. R. Albrecht, R. N. Hook, & H. A. Bushouse, ASP Conf. Ser., 145, 53
Widemann, T., Sicardy, B., Dusser, R., et al. 2009, Icarus, 199, 458
Zacharias, N., Urban, S. E., Zacharias, M. I., et al. 2004, AJ, 127, 3043
Zacharias, N., Finch, C. T., Girard, T. M., et al. 2013, AJ, 145, 44

[10] These new determinations are explicitly indicated on the site http://devel2.linea.gov.br/braga.ribas/campaigns/ when they are made.